

Silicon nanocrystal formation in annealed silicon-rich silicon oxide films prepared by plasma enhanced chemical vapor deposition

N. Daldosso,^{a)} G. Das, S. Larcheri, G. Mariotto, G. Dalba, and L. Pavese
Dipartimento di Fisica, Università di Trento, via Sommarive 14, 38050 Povo (Trento), Italy

A. Irrera and F. Priolo
MATIS CNR-INFN and Dipartimento di Fisica e Astronomia, Università di Catania, via Santa Sofia 64, 95123 Catania, Italy

F. Iacona
CNR-IMM, Sezione di Catania, Stradale Primosole 50, 95121 Catania, Italy

F. Rocca
CNR-IFN, Sezione "ITC-CeFSA" di Trento, via Sommarive 18, 38050 Povo (Trento), Italy

(Received 3 January 2007; accepted 10 April 2007; published online 5 June 2007)

Silicon-rich silicon oxide films deposited by plasma enhanced chemical vapor deposition with different total Si contents (from 39 to 46 at. %) have been annealed at increasing temperature (up to 1250 °C) in order to study the Si nanocrystal (Si-nc) nucleation as well as the structural changes induced in the amorphous embedding matrix. The comparison between x-ray absorption measurements in total electron yield mode, Raman spectroscopy, and photoluminescence spectra allowed us to gain insight about the Si nanocrystal formation, while the chemical composition and the nature of chemical bonds into the oxidized matrix was studied by Fourier transform infrared spectroscopy. A comprehensive picture of the nucleation process has been obtained, demonstrating the active role played by the hydrogen and nitrogen atoms in the formation of Si-nc and in the thermally induced evolution of the deposited films. © 2007 American Institute of Physics.

[DOI: [10.1063/1.2740335](https://doi.org/10.1063/1.2740335)]

I. INTRODUCTION

In the last years, important advancements in the study of silicon nanocrystals (Si-nc) embedded in amorphous silica thin films (*a*-SiO₂) have been motivated by the potentiality of Si-nc in active light sources and in memory devices.¹⁻⁴

Amorphous silicon-rich silicon oxide (SRO) films may be produced by different techniques, i.e., plasma enhanced chemical vapor deposition (PECVD), ion implantation, sputtering, sol gel, etc. Among these, PECVD is widely used since it is generally present in a complementary metal oxide semiconductor (CMOS) processing line and warrants a good control of the film composition (Si content and film thickness), good adhesion to substrate, low deposition defects, and low compressive stress in the deposited film. In these films, the excess Si is dispersed in the amorphous silica matrix. Hence, nucleation of Si nanoaggregates is induced by a high temperature annealing. Depending on the deposition conditions and on the temperature and duration of the annealing processes, it is possible to obtain amorphous aggregates or crystalline Si-nc with different sizes and distributions embedded into an amorphous SiO_x matrix, whose structure (stoichiometry and defect content) is also determined by the annealing processes.

The structure of SRO films is usually described by a network of fourfold and twofold bonded Si and O atoms, respectively. The random-mixture model⁵ (RMM) assumes a simple mixture of Si and SiO₂, while the random bonding

model⁶ (RBM) is based on the assumption of a statistical distribution of Si-Si and Si-O bonds. RMM focuses on the structure and chemistry of the film by considering the two more stable structural phases in the sample (Si aggregates and amorphous SiO₂). RBM focuses on the different chemical bonds of Si (i.e., with Si and/or O). The SRO film is described as a mixture of all the Si oxidation states under the form of Si-Si_xO_{4-x} tetrahedra (0 < *x* < 4). Experimentally, SRO films show characteristic features intermediate between the predictions of the two models. Hence to properly model the optical properties of SRO films, a complete structural characterization is needed. As a function of the process parameters (e.g., the annealing temperature) the amount of Si atoms progressively segregated into silicon clusters, the evolution of the size, the distribution and crystalline nature of the silicon clusters, and the chemical composition and structure of the host matrix have to be determined.

In a previous work,⁷ we have provided evidences of the presence of 1 nm thick interface region (stressed oxide) which coats the Si-nc. Experimental x-ray absorption studies and *ab initio* density functional calculations pointed out that this modified substoichiometric SRO region participates to the light emission process and plays an important role in determining the optoelectronic properties of the system. Successively, the process of Si-nc formation in thermally annealed SRO films has been studied using the energy filtered transmission microscopy (EFTEM) technique.⁸

In PECVD samples due to the use of N₂O as precursor, the picture is even more intriguing because of the presence of

^{a)}Electronic mail: daldosso@science.unitn.it

nitrogen atoms incorporated during the deposition process. The presence of nitrogen atoms in the amorphous SiO_x network introduces defect states localized at Si–N bonds. These are active in hole trapping and transport, and strongly influence the balance between radiative and nonradiative decay processes.^{9–12} In spite of the research activity on the role of N in $\text{SiO}_x\text{N}_y\text{:H}$ samples,^{9,11,13,14} a clear compositional and structural picture is still lacking, particularly about the role of the annealing temperature. Based on x-ray absorption spectroscopy (XAS) measurements of PECVD SRO samples annealed at high temperature (1250 °C), we have shown that the Si excess partially segregates forming Si-nc and partially remains into the amorphous matrix bonded to O and N atoms.¹⁵ Thus the matrix cannot be simply considered as amorphous silica but rather as a substoichiometric Si oxynitride amorphous phase. This fact has been confirmed by EFTEM.⁸ The complexity of the processes induced by thermal annealing and their dependence on silicon excess and N and H impurity content has been the object of some recent papers.^{9,16,17} It is worth noting here that the formation of amorphous Si oxynitride modifies the optical properties as confirmed by refractive index measurements on the same samples,¹⁸ and lowers the structural strains with respect to stoichiometric amorphous SiO_2 .¹¹

In a previous paper⁸ on the same series of samples, TEM studies pointed out the presence of Si nanocrystals after annealing at high temperature (above 1000 °C). In this paper, we report on the results of a systematic characterization of PECVD SRO films as a function of the annealing temperature. A multitechnique approach based on Raman scattering, photoluminescence (PL), XAS in total electron yield (TEY) mode at the Si k edge, and Fourier transform infrared (FT-IR) absorption spectroscopy has been used. The chemical composition of the films, the nature of chemical bonds in the matrix and their structural evolution, the formation of amorphous Si nanoaggregates at low annealing temperature, and the nucleation of Si nanocrystals at high annealing temperatures have been investigated.

II. EXPERIMENT

Silicon nanocrystals have been produced by thermal annealing of SRO films prepared by PECVD. The substrates were 5 in. (100) Czochralski silicon (1.5–4 Ω cm) or quartz wafers. The source gases used were high purity (99,99% or higher) SiH_4 and N_2O . The $\text{N}_2\text{O}/\text{SiH}_4$ flow ratio γ has been varied between 6 and 15 in order to obtain SRO films with different Si content. The film thickness ranges from 200 to 1000 nm. During the deposition, both the total gas flow and the total pressure were kept constant [about 140 SCCM (SCCM denotes cubic centimeter per unit at STP) and 6×10^{-2} Torr, respectively]. Due to the use of N_2O as one of the gaseous precursors, the amorphous matrix contains about 10% of nitrogen.³ We have investigated samples with different Si content (39, 42, 44, and 46 Si at. %), annealed for 1 h at different temperatures (from 500 up to 1250 °C) by various spectroscopic techniques: Raman scattering, FT-IR absorption, x ray absorption, and PL.

XAS spectra were measured at Super-ACO (LURE) on

the SA32 soft x-ray beamline. The total yield of electrons (TEY mode) escaping from the sample after the x-ray absorption at the Si k edge was monitored by detecting the drain current through a nanoamperometer. By scanning the x-ray energy (with a resolution of 0.2 eV) in the near edge region, it has been possible to clearly identify the main features corresponding to different local environments of silicon, because they are well separated in energy: the absorption k edge of Si both in the crystalline (c -Si) and amorphous (a -Si) phase is centered at 1839 eV, while for Si atoms in silica the edge is up-shifted to about 6 eV, showing a very sharp and intense peak whose maximum is at about 1847 eV.¹⁵ The sampling depth of TEY technique at Si k -edge energy is about 100 nm for both c -Si and SiO_2 ,¹⁹ while most of the signal is originated from the absorbing atoms in the near-surface region. The homogeneity in depth of the studied samples was previously controlled by Rutherford backscattering spectrometry (RBS), as documented in Ref. 3.

FT-IR absorption measurements were carried out at room temperature, under vacuum conditions, in transmission mode, in the spectral range between 4000 and 400 cm^{-1} using a JASCO FT/IR-660 plus spectrometer having a ceramic source, a KBr beam splitter, and a thermoelectrically cooled tri-glycine-sulphate (TGS) detector. All the IR spectra were collected with a resolution of 4 cm^{-1} using Si wafer as a reference. The baseline has been subtracted from all the spectra and the intensity was normalized to the film thickness.

Depolarized Raman spectra were measured at room temperature by means of an Ar^+ -ion laser, a double monochromator (Jobin Yvon, model Ramanor HG2-S) equipped with holographic gratings (2000 lines/mm), and a photomultiplier tube (RCA model 31034 A-02), operated in photon counting mode. The spectra were excited by the 488 nm laser line, the laser power at the sample surface being of 100 mW. The incident laser beam was polarized within the scattering plane (H) and was incident onto the sample surface at the Brewster angle of Si to maximize light intensity within the sample; the scattered radiation polarized in vertical plane (V) was analyzed. All the measurements were done in vacuum to avoid the superposition of the Raman lines due to air below 160 cm^{-1} .

PL was excited by an Ar^+ laser (488 nm emission line at 20 mW) focused to a spot size of 1 mm^2 , emission was analyzed by a single spectrometer interfaced to a charge coupled device (CCD) detector. PL spectra have been corrected for the spectral response of the optical setup.

III. RESULTS AND DISCUSSIONS

A. X-ray absorption

In Fig. 1(a) x-ray absorption near edge structure spectra collected in total electron yield (TEY-XANES spectra) at the Si k edge of the as deposited samples are shown as a function of the Si content (39, 42, 44, and 46 at. %). It is worth noting that the film structure changes as the Si content increases and different absorption features can be recognized. Apart from the well known absorption features at about 1839 and

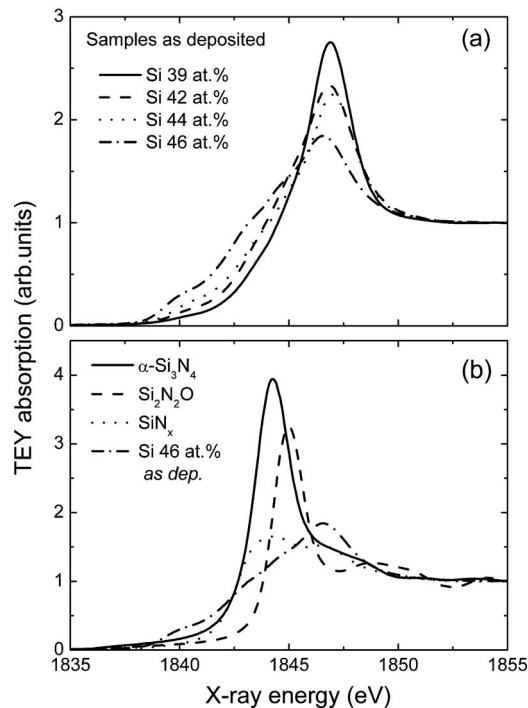


FIG. 1. TEY absorption spectra of as deposited SRO samples (a) and reference samples (b). Spectra have been normalized at about 1855 eV.

1847 eV (due to the absorption edges of Si in silicon and in silica, respectively),¹⁵ other features are present in the energy range from about 1842 to 1845 eV. They become more pronounced with increasing the Si content. We assign these absorption structures to segregated species containing Si–N bonds, which are probably present in different structural configurations, thus resulting in a continuous broad absorption feature. This is supported by the comparison presented in Fig. 1(b), where the XAS spectra of various nitrides are shown: a nonstoichiometric SiN_x sample (with different local structural configurations of Si–N bonds) and two crystalline reference compounds (silicon nitride Si₃N₄ and silicon oxynitride Si₂N₂O). Crystalline nitride samples show sharp absorption peaks at 1843.5 eV (Si₃N₄) and at 1844.6 eV (Si₂N₂O). At odds with what is shown by SRO, in these nitrides no absorption structures at 1839 eV are measured, only a weak featureless absorption tail. Thus, the contribution in the XANES spectra of SRO samples growing up at 1839 eV with a maximum at about 1841 eV indicates the presence of short-range clustering of Si atoms tetraordinated to Si as it occurs in *c*-Si or *a*-Si. These tetraordinated silicon arrangements are detected thanks to the short-range high sensitivity of XAS measurements.

To monitor how the annealing promotes the thermal nucleation of silicon nanoclusters while it modifies the matrix, we have measured TEY-XANES spectra as a function of the annealing temperature. Figure 2(a) compares the spectra of the as deposited and 1250 °C annealed samples for various Si content. Figure 2(b) shows the annealing temperature evolution of the TEY-XANES spectra for a representative sample with 44 at. % of Si. Whereas the absorption features of the as deposited samples have different shape, position, and intensity, all the TEY-XANES spectra of the 1250 °C

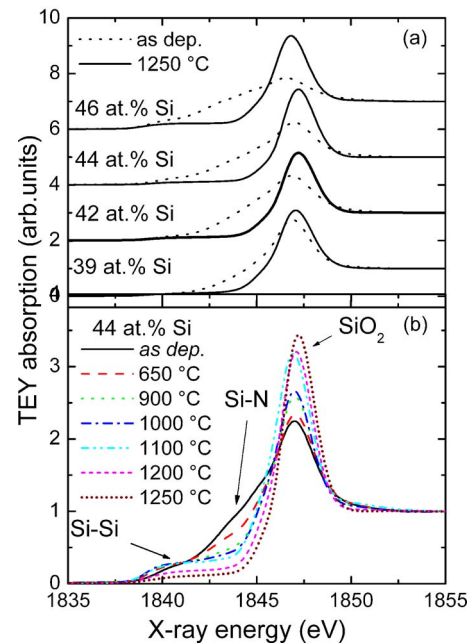


FIG. 2. (Color online) TEY absorption spectra of (a) as deposited and annealed (1250 °C) films for different Si content (39, 42, 44, and 46 at. %) and (b) sample with 44 at. % of Si as a function of the annealing temperature.

annealed samples are very similar: two main absorption structures related to Si-nc (at 1841 eV) and to the silica matrix (at 1847 eV). The increase of the nominal Si content in the samples results in an increase of the absorption at 1841 eV with respect to the normalized matrix absorption at 1850 eV. From Fig. 2(b), we may observe that during the 650 °C annealing most of the Si-cluster nucleation is already obtained as measured by the strengthening of the 1841 eV absorption. Only small changes occur when the annealing temperature is increased up to 1100 °C (we will discuss later the very high temperature behavior). It is worth noting that the crystallization process of the Si clusters, as well as changes in the Si-nc mean size, cannot be monitored by the XANES spectra: we can only study the evolution of the relative number of Si atoms that are contributing to the absorption feature at about 1841 eV. A decrease of the Si-nc related absorption at 1841 eV is observed in some samples after high temperature annealing. This could be due to the structural modification of the SiN_xO_y amorphous matrix and to Si depletion at the surface of the SRO. It is well known that surface oxidation might occur during the thermal treatment.¹⁷ It is quite difficult to quantitatively assess the influence of the surface oxidation on the absorption decrease because the relative content of Si-nc is low and a nitride absorption tail overlaps to the Si-nc absorption at 1841 eV.

The Si–N bonds related broad absorption structures in the energy range from about 1842–1845 eV weaken significantly with the increase of the annealing temperature. The analysis of the derivative plots shows that these contributions are negligible already after annealing at 1000 °C. By comparing the spectra of the different samples reported in Fig. 2(a), it is clear that the presence of Si–N bonds is more relevant for large Si content. Since the total nitrogen content in PECVD SRO samples is neither strongly depending on the

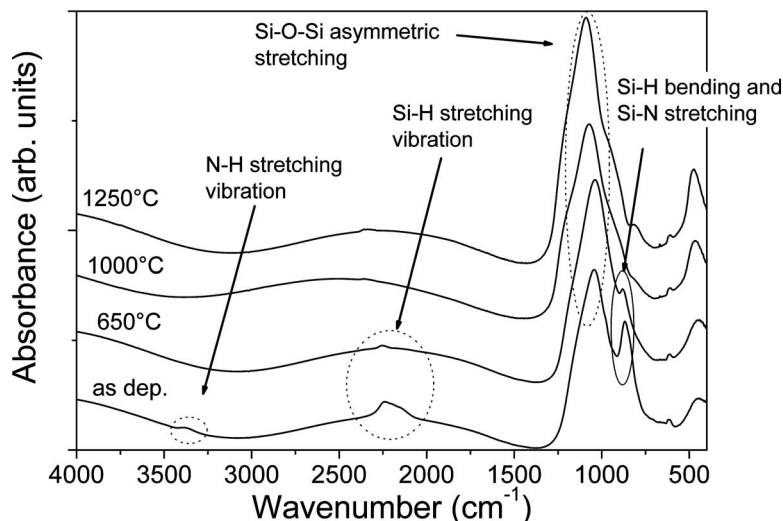


FIG. 3. FT-IR spectra of sample with 46 at. % of Si as deposited and annealed at different temperatures. The main absorption peaks are labeled.

Si content nor on the annealing temperature,³ the TEY-XANES spectra evolution can be interpreted as a temperature activated breaking and rearrangement of Si–N bonds in the amorphous matrix. The silicon nitride bonds of either SiN or SiNO small clusters (which are responsible for the TEY signals between 1842 and 1845 eV in Figs. 1 and 2) tend to be weak and then break with increasing the annealing temperature. The nitrogen is dispersed within the amorphous oxide matrix forming a more homogeneous Si oxynitride phase, while the excess Si forms the Si nanoclusters, whose nature (amorphous or crystalline) cannot be discriminated from x-ray absorption measurements. As we will see in the following, IR spectroscopy is able to follow in detail this process showing also a role played by hydrogen atoms (to which the XANES measurements are insensitive).

At high annealing temperatures (>900 °C), the amorphous oxide matrix composition changes to a stoichiometric phase. This is well documented by the changes of the TEY-XANES spectra at energies higher than 1845 eV, where the silica absorption is dominated by an intense sharp peak at 1847 eV [see Fig. 2(b)]. As the temperature increases, this peak becomes more intense and sharp, suggesting a gradual evolution towards a homogeneous structure similar to amorphous silica. For fixed annealing temperature, the amplitude of the silica absorption peak is lower, while the full width at half maximum (FWHM) is larger as the Si content increases: the larger the Si content the greater the distortion of this peak [Fig. 2(a)]. The peak distortion is due to nonhomogeneity and disorder inside the matrix, owing to the presence of Si–N bonds. In the high temperature range, TEY-XANES spectra monitor the final stage of the annealing process, when the clustering of Si in excess has already come to an end and the dominant effect appears to be the relaxation of residual stresses in the Si oxynitride matrix. It is worth noting that for high annealing temperature the amorphous matrix can be described as an oxynitride phase where nitrogen atoms are substitutes of oxygen ones.¹⁵

B. Fourier transform infrared absorption

FT-IR absorbance spectra of the representative sample with 46 at. % of Si are shown in Fig. 3 for various annealing

temperatures. We observe peaks at about 450, 870, 1050, 2200, and 3370 cm^{-1} , which are attributed to Si–O–Si vibration in rocking mode, Si–H bending and Si–N stretching vibration modes, Si–O–Si asymmetric stretching vibration, Si–H stretching mode, and N–H stretching vibration mode, respectively.²⁰ For the as deposited sample, the peak at about 2200 cm^{-1} due to the Si–H stretching mode consists of three main components at 2238, 2200, and 2145 cm^{-1} , which are due to the presence of different structural units of $\text{HSi}-(\text{Si}_{3-n}\text{O}_n)$. By considering the random bonding model,⁶ these peaks can be attributed to Si–H stretching vibrations in $\text{O}_3\text{Si}-\text{H}$, $\text{SiO}_2\text{Si}-\text{H}$, and $\text{Si}_2\text{OSi}-\text{H}$ structural units, respectively. It is evident from Fig. 3 that all the H related features decrease rapidly with increasing the annealing temperature as hydrogen out diffuses.

The evolution of the main absorption bands at low wave numbers is worth a more detailed discussion (see Fig. 4). For the as-deposited sample, three major absorption peaks are present at 1044, 864, and 460 cm^{-1} , which can be attributed to the Si–O–Si asymmetric stretching, Si–H bending vibration, and Si–O rocking vibration mode, respectively. Nonstoichiometry in SRO is observed in the shift of the Si–O modes with respect to their positions in pure thermally grown SiO_2 which shows the Si–O vibrational frequencies at 1080, 810, and 465 cm^{-1} .^{20,21} Annealing up to 900 °C causes variations in the FT-IR spectra with a significant decrease of the H related vibrations and a weak high wave number shift of the main peak. H outdiffusion and Si clustering are responsible of these behaviors.

As the annealing temperature increases further, the only detectable contributions to the IR spectra are those related to Si–O bonds. In addition, the main peak due to the Si–O–Si stretching shifts to 1090 cm^{-1} at 1250 °C. At low annealing temperatures, as those shown in Fig. 4(a), the shift of the Si–O–Si stretching mode is probably due to local structural rearrangements, e.g., densification, following the outdiffusion of hydrogen and the melting down of the Si–N bonds.²²

We may also note that, the width of Si–O–Si stretching absorption peak reduces with increasing the annealing temperature. Its value at high annealing temperature is, however, larger than what has been observed in good quality thermally

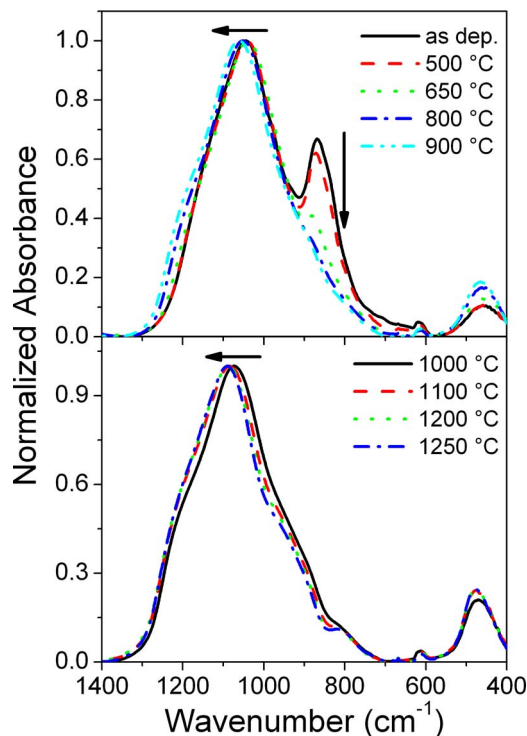


FIG. 4. (Color online) Normalized FT-IR absorption spectra of sample with 46 at. % of Si as a function of the annealing temperature in the range of 400–1400 cm^{-1} . Top panel: low temperature range up to 900 °C. Bottom panel: high temperature range from 1000 up to 1250 °C. The arrows are a guide to the eye to follow the evolution of the spectra with the raising of the temperature.

grown SiO_2 samples: 90 cm^{-1} at 1250 °C versus about 80 cm^{-1} . The broadening of the Si–O–Si stretching absorption peak is due to the strains induced by the Si clustering.

These general trends are observed also in the other Si content SRO samples. We have found that the relevance of strains and defects due to the formation of a high density of Si–Si bonds in the Si-nc increases with the increase of Si content.²³

C. Raman measurements

Raman spectra of the representative sample with 46 at. % of Si as a function of the annealing temperature are reported in Fig. 5. The as-deposited sample shows a very flat Raman spectrum with a main sharp peak at about 521 cm^{-1} due to the contribution of the *c*-Si substrate. In fact, in similar samples deposited on quartz substrate this peak was absent. Annealing changes the Raman spectra with two main features: a peak centered between 515 and 518 cm^{-1} due to the Si-nc precipitation in the oxide matrix,²⁴ and the appearance of two broad and asymmetric bands centered at about 475 cm^{-1} (TO mode) and at about 160 cm^{-1} (TA mode). In Fig. 5 the Si-nc peak is masked by the substrate contribution. However, a low frequency tail develops on the *c*-Si contribution at high annealing temperatures (see, e.g., spectrum for 1100 °C), which for further annealing merges into the *c*-Si contribution.^{25,26} The evolution of the peak at about 520 cm^{-1} is quite standard for Si-nc and reveals the formation of crystalline Si-nc. To point out the presence of Si-nc peak, Fig. 6 reported the Raman spectrum of the sample

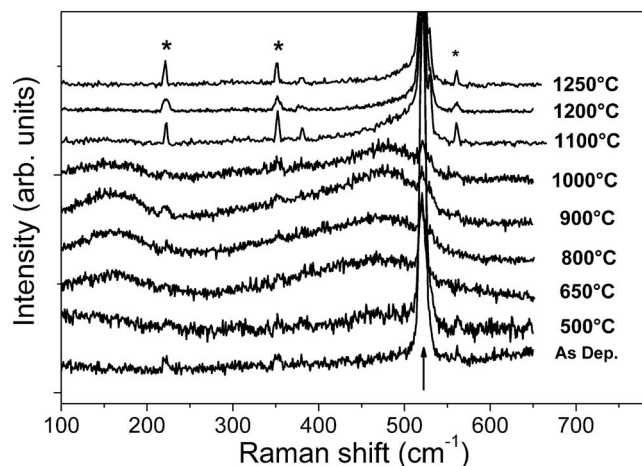


FIG. 5. Raman spectra for sample with 46 at. % of Si content as a function of the annealing temperature. Arrow at 521 cm^{-1} indicates the *c*-Si peak due to the substrate and * indicates the plasma lines of 488 nm argon laser.

annealed at 1100 °C after subtracting the substrate contribution.²⁷ The contribution of *a*-Si (fitted by a Gaussian distribution centered at 480 cm^{-1} with a FWHM of about 70 cm^{-1}) and of Si-nc (fitted by using the confinement model²⁸ and resulting in a peak at 515 cm^{-1}) are evident. The peak at 515 cm^{-1} corresponds to a Si-nc size of about 5 nm, which is in good agreement with EFTEM measurements.⁸

What is interesting is the appearance of the broad bands at low frequencies which are observed for samples annealed at temperatures higher than 600 °C but lower than 1100 °C. These features are typical of amorphous Si nanoclusters.²⁹ Hence evidences of phase separation and clustering at temperatures as low as 650 °C are observed here. Moreover, the broad band at 475 cm^{-1} sharpens on increasing the annealing temperature up to 1000 °C and disappears on further annealing, thus suggesting an increase in the ordering of the amorphous Si nanoclusters and a transition from amorphous to crystalline clusters.³⁰ These findings are also in agreement with previous EFTEM data.⁸ In addition, these structural changes are also reflected in the low frequency band. The broad peak observed at about 160 cm^{-1} grows with the in-

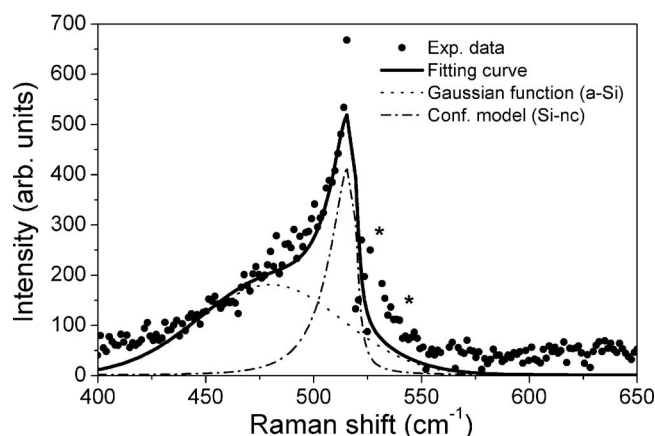


FIG. 6. Raman spectra of sample with 46 at. % of Si content annealed at 1100 °C after subtraction of the substrate contribution. The contribution of *a*-Si is fitted by a Gaussian distribution centered at 480 cm^{-1} width and that of Si-nc is fitted by using the confinement model.

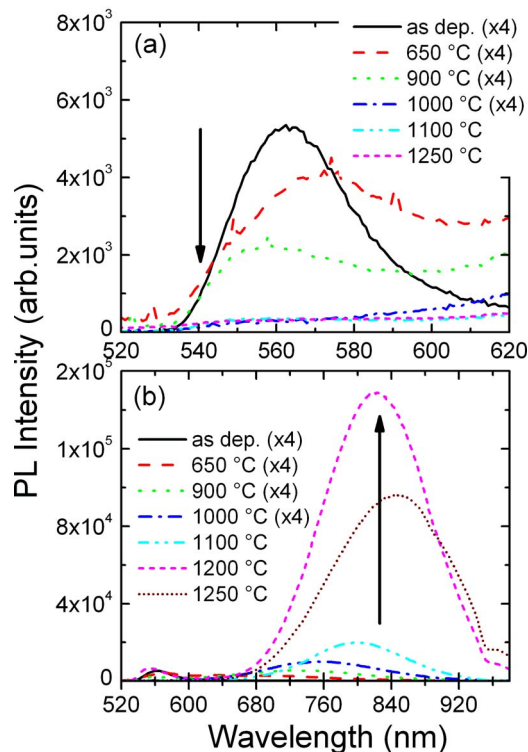


FIG. 7. (Color online) PL spectra (obtained using the 488 nm emission line of an Ar⁺ laser) of 42 at. % Si sample as a function of the annealing temperature. Panel (a) reports the 520–620 nm region to better clarify the behavior of the short wavelength band, and panel (b) reports the whole wavelength range. The arrows are a guide to the eye to follow the evolution of the spectra with the raising of the temperature.

crease of the annealing temperature up to 800 °C and starts diminishing on further annealing. The behaviors of the broad bands reveal an increase in local ordering of the silicon amorphous structure with annealing temperature up to 1000 °C. Above this temperature, both TO and TA bands disappear due to the formation of Si nanocrystals.³¹

Raman spectra were also performed on the other samples with 42 and 44 at. % Si content. Similar but less evident trends were observed, due to the lower Si content.

D. Photoluminescence

PL spectra as a function of the annealing temperature are shown in Fig. 7 for sample with 42 at. % of Si. The as prepared and 650 °C annealed samples show only a faint PL band at about 550–580 nm that weakens after further annealing [see Fig. 7(a)]. Light emission in this range can be due to radiative states related to local defects in the amorphous matrix. However, the comparison between TEY-XANES and PL spectra suggests that this luminescence band may be due to the small Si nitride clusters segregated in the amorphous matrix, in samples annealed at low temperature.^{9,11} As the annealing temperature increases, TEY-XANES have documented the disappearing of the small Si nitrides aggregates, and PL spectra document the parallel disappearing of the related band, because the amorphous matrix modifies reducing the dangling bonds and forming a Si oxynitride matrix.

Only for annealing temperatures higher than 1100 °C, an intense PL band rises at about 800–900 nm. This band shifts towards higher wavelength due to the growing of Si-nc size and becomes very intense in samples annealed at temperatures higher than 1100 °C [Fig. 7(b)]. This band is the expected contribution due to Si nanocrystals, deeply studied in previous papers for the samples annealed at 1250 °C.⁷ Note that the appearance of this band correlates with the crystallization of the amorphous silicon clusters. It can be argued that the low PL bands at about 750–770 nm shown for 900 and 1000 °C annealing temperature may be attributed to light emission from small amorphous silicon clusters.³² However, it is out of the goal of this paper to assess if the silicon nanoaggregates are completely crystalline or a cap shell is amorphous,³³ and whether radiative recombination can occur also in very small silicon clusters.³²

IV. CONCLUSIONS

The main findings of the various spectroscopic techniques we used to investigate the behavior of the SRO films as a function of the annealing temperature can be summarized as follows:

- XAS measurements indicate that the as deposited samples are formed by a nonhomogeneous amorphous matrix where the Si excess and the presence of N atoms cause the formation of disordered silicon-rich and nitrogen-rich nanoaggregates. Once the annealing temperature is increased the N-related species decrease and vanish after 1000 °C; the amorphous silica matrix modifies towards a homogeneous Si oxynitride, having a quite low nitrogen content and, therefore, a composition very similar to pure SiO₂; a rearrangement of the matrix stoichiometry occurs (mainly related to a redistribution of N); Si nanoclusters grow and separate from the embedding matrix. (However, small and amorphous Si nanoclusters are present also for very low annealing temperatures.)
- FT-IR measurements show a relevant contribution of O, N, and H vibrational modes in the as-deposited samples. With increasing the annealing temperature it is observed that the N–H and Si–H bond densities decrease due to the outdiffusion of H. A positive role of H is observed in passivating dangling bonds in the defect substoichiometric matrix. H reduces also internal strain in the as-deposited films.³⁴ The evolution of the Si–O–Si asymmetric frequency reflects the H outdiffusion and the increase of the strain in the film at intermediate annealing temperatures. At high annealing temperature the Si–O–Si vibration becomes similar to the one of pure SiO₂ confirming the quality of the dielectrics at high annealing temperature as observed by XAS.
- The temperature evolution of the Raman measurements points out the presence of amorphous Si nanoclusters at moderate temperatures (500–1000 °C), which start ordering as annealing temperature is increased, and the crystallization of Si nanoclusters with annealing at higher temperature (>1000 °C).

- Photoluminescence measurements show that defect silica or N-rich nanoclusters related emissions are the only one present in the emission spectra of as-deposited or low temperature annealed samples; when evidences by Raman exist of the formation of amorphous silicon nanoclusters a weak emission band develops in the red; this band strengthens and further redshifts when crystalline Si-nc develops at high annealing temperature.

In conclusion, the analysis of TEY-XANES, FT-IR, Raman, and PL data has allowed us to assess the structural evolution and nucleation of Si-nc in SRO films produced by PECVD, as a function of the annealing temperature. This cannot be modeled by a simple phase separation between Si and silica but follows a more complicated scheme, where hydrogen and nitrogen atoms play a key role in the formation of Si clusters and in the structural evolution of the host matrix.

Raman, PL, and XAS measurements show that, within the SRO film, the excess Si in the matrix precipitates to form amorphous Si nanoclusters at moderate annealing temperature ($T \leq 1000$ °C). In samples annealed at higher temperatures, the process of crystallization of Si nanocrystals embedded in a Si oxynitride network takes place, where nitrogen is substitutional of oxygen. No separation of a clear Si nitride phase is observed after high temperature annealing.

ACKNOWLEDGMENTS

The authors acknowledge the support by the Training and Mobility of Researchers (TMR) Programme of the European Community for measurements at the LURE Laboratories (Orsay-France). Trento has been supported by the EC Project No. NMP-505285 SEMINANO. One of the authors (G. D.) acknowledges the financial support of the Italian Ministry of External Affairs.

¹L. Pavesi, L. Dal Negro, C. Mazzoleni, G. Franzò, and F. Priolo, *Nature (London)* **408**, 440 (2000); L. Dal Negro *et al.*, *Physica E (Amsterdam)* **16**, 297 (2003); J. Ruan, P. M. Fauchet, L. Dal Negro, M. Cazzanelli, and L. Pavesi, *Appl. Phys. Lett.* **83**, 5479 (2003); L. Khriachtchev, M. Rasanen, S. Novikov, and J. Sinkkonen, *Appl. Phys. Lett.* **79**, 1249 (2001).

²*Towards the First Silicon Laser*, edited by L. Pavesi, S. Gaponenko, and L. Dal Negro, NATO Science Series II: Mathematics, Physics, and Chemistry

Vol. 93 (Kluwer Academic, Dordrecht, 2003).

³F. Iacona, G. Franzò, and C. Spinella, *J. Appl. Phys.* **87**, 1295 (2000).

⁴M. Cazzanelli *et al.*, *J. Appl. Phys.* **96**, 3164 (2004).

⁵R. J. Temkin, *J. Non-Cryst. Solids* **17**, 215 (1975).

⁶H. R. Philipp, *J. Non-Cryst. Solids* **8-10**, 627 (1972).

⁷N. Daldosso *et al.*, *Phys. Rev. B* **68**, 085327 (2003).

⁸F. Iacona, C. Bongiorno, C. Spinella, S. Boninelli, and F. Priolo, *J. Appl. Phys.* **95**, 3723 (2004).

⁹X. Y. Chen, Y. F. Lu, L. J. Tang, Y. H. Wu, B. J. Cho, X. J. Xu, J. R. Dong, and W. D. Song, *J. Appl. Phys.* **97**, 014913 (2005).

¹⁰C. Ance, F. D. Chelle, J. P. Ferraton, G. Leveque, P. Ordejon, and F. Yndurain, *Appl. Phys. Lett.* **60**, 1399 (1992).

¹¹K. J. Price, L. E. McNeil, A. Suvkanov, E. A. Irene, P. J. MacFarlane, and M. E. Zvanut, *J. Appl. Phys.* **86**, 2628 (1999).

¹²S. Hasegawa, S. Sakamori, M. Futatsudera, T. Inokuma, and Y. Kurata, *J. Appl. Phys.* **89**, 2598 (2001).

¹³Z. H. Lu, S. P. Tay, R. Cao, and P. Pianetta, *Appl. Phys. Lett.* **67**, 2836 (1995).

¹⁴E. C. Carr, K. A. Ellis, and R. A. Buhrman, *Appl. Phys. Lett.* **66**, 1492 (1995).

¹⁵G. Dalba, N. Daldosso, P. Fornasini, R. Grisenti, L. Pavesi, F. Rocca, G. Franzò, F. Priolo, and F. Iacona, *Appl. Phys. Lett.* **82**, 889 (2003).

¹⁶T. Ehara and S. Machida, *Thin Solid Films* **346**, 275 (1999).

¹⁷V. Mulloni, P. Bellutti, and L. Vanzetti, *Surf. Sci.* **585**, 137 (2005).

¹⁸G. Vijaya Prakash, M. Cazzanelli, Z. Gaburro, L. Pavesi, F. Iacona, G. Franzò, and F. Priolo, *J. Mod. Opt.* **49**, 719 (2002).

¹⁹A. Erbil, G. S. Cargill III, R. Frahm, and R. F. Boehme, *Phys. Rev. B* **37**, 2450 (1988).

²⁰A. Sassella *et al.*, *J. Vac. Sci. Technol. A* **15**, 377 (1997).

²¹F. Rochet, G. Dufour, H. Roulet, B. Pelloie, J. Perriere, E. Fogarassy, A. Slaoui, and M. Froment, *Phys. Rev. B* **37**, 6468 (1988).

²²G. Lucovsky, M. J. Mantini, J. K. Srivastava, and E. A. Irene, *J. Vac. Sci. Technol. B* **5**, 530 (1987).

²³G. Mariotto, G. Das, A. Quaranta, G. Della Mea, F. Corni, and R. Tonini, *J. Appl. Phys.* **97**, 113502 (2005).

²⁴N. Daldosso *et al.*, *Mater. Res. Soc. Symp. Proc.* **770**, 45 (2003).

²⁵D. Nesheva, C. Raptis, A. Perakis, I. Bineva, Z. Aneva, Z. Levi, S. Alexandrova, and H. Hofmeister, *J. Appl. Phys.* **92**, 4678 (2002).

²⁶G. Mariotto, F. Ziglio, and F. L. Freire, Jr., *J. Appl. Phys.* **78**, 3335 (1995).

²⁷L. Khriachtchev, O. Kilpelä, S. Karirinne, J. Keränen, and T. Lepistö, *Appl. Phys. Lett.* **78**, 323 (2001).

²⁸H. Campbell and P. M. Fauchet, *Solid State Commun.* **58**, 739 (1986).

²⁹V. N. Denisov, B. N. Mavrin, F. A. Pudonin, and E. A. Vinogradov, *Sov. Phys. Solid State* **32**, 2174 (1990).

³⁰R. L. C. Vink, G. T. Barkema, and W. F. van der Weg, *Phys. Rev. B* **63**, 115210 (2001).

³¹G. Mariotto, F. Ziglio, and F. L. Freire, Jr., *J. Appl. Phys.* **78**, 3335 (1995).

³²L. Khriachtchev, M. Rasanen, S. Novikov, and L. Pavesi, *Appl. Phys. Lett.* **85**, 1511 (2004).

³³A. Meldrum, A. Hryciw, A. N. MacDonald, C. Blois, K. Marsh, J. Wang, and Q. Li, *J. Vac. Sci. Technol. A* **24**, 713 (2006).

³⁴R. Tsu, J. Gonzalez-Hernandez, J. Doehler, and S. R. Ovshinsky, *Solid State Commun.* **46**, 79 (1983).